A glutamatergic DRN–VTA pathway modulates neuropathic pain and comorbid anhedonia-like behavior in mice

Xin-Yue Wang[1*], Wen-Bin Jia[1*], Xiang Xu[1], Rui Chen[1], Liang-Biao Wang[1], Xiao-Jing Su[1], Peng-Fei Xu[1], Xiao-Qing Liu[2], Jie Wen[3], Xiao-Yuan Song[4], Yuan-Yuan Liu[5], Zhi Zhang[4†], Xin-Feng Liu[1†] and Yan Zhang[1†]

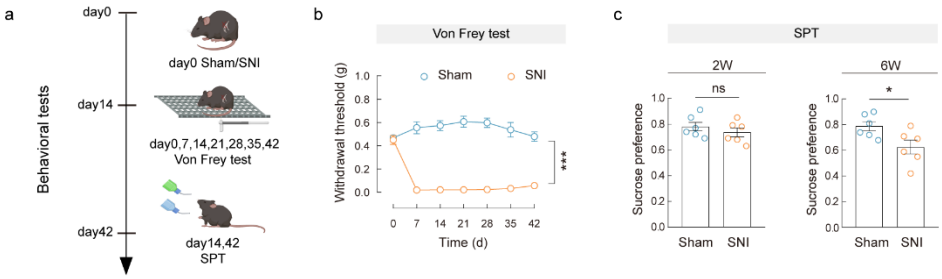

Supplementary Fig 1. Time course of SNI-induced mechanical hypersensitivity and comorbid anhedonia-like behavior.

a, Schematic of the experimental design. **b**, **c**, Performance of mice treated with sham or SNI in von Frey test (**b**: Sham, n = 6; SNI, n = 5 mice. $P = 0.0009$) and SPT (**c**: Sham, n = 6; SNI, n = 6 mice. 2W $P = 0.3892$; 6W $P = 0.0312$). Significance was assessed by two-way ANOVA followed by Bonferroni's multiple comparisons test in (**b**), and two-tailed unpaired Student's *t*-test in (**c**). All data are presented as the mean ± s.e.m. $*P < 0.05$, $***P < 0.001$, not significant (ns). Details of the statistical analyses are presented in Supplementary Data 1. Created with BioRender.com (**a**).

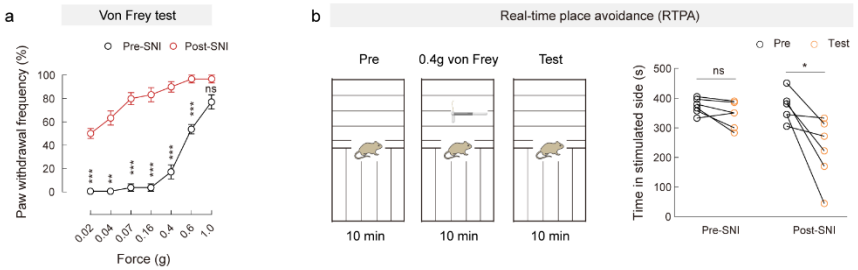

Supplementary Fig 2. Mechanical withdrawal frequency to von Frey filament and RTPA test before and after SNI.

a, Statistical data for mechanical withdrawal frequencies to von Frey filaments applied on the hind paw in *C57* mice before (pre-SNI) and after (post-SNI 2W) SNI. **b**, Experimental design of real-time place avoidance (RTPA) test (left) and quantification of RTPA before (Pre) and after (Test) training of the pre-SNI ($P = 0.0995$) or post-SNI 2W ($P = 0.0237$) mice (right). n = 6 mice per group in panels (**a**, **b**). Significance was assessed by two-way ANOVA followed by Bonferroni's multiple comparisons test in (**a**) and two-tailed paired Student's *t*-test in (**b**). All data are presented as the mean ± s.e.m. $*P < 0.05$, $**P < 0.01$, $***P < 0.001$, not significant (ns). Details of the statistical analyses are presented in Supplementary Data 1.

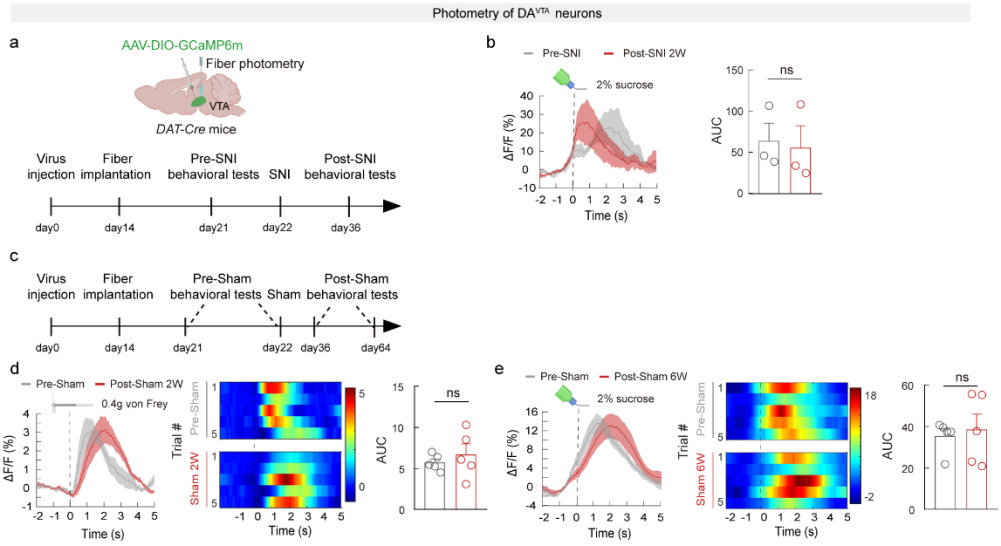

Supplementary Fig 3. Ca^{2+} signal of DA^{VTA} neurons in *DAT-Cre* mice.

a, Schematic of the experimental design and schematic diagram of fiber photometry of DA^{VTA} neurons. **b**, Averaged responses (left) and AUC during 0-5 s (right) showing Ca^{2+} responses evoked by sucrose licking in pre- and post-SNI 2W mice. (n = 3 mice. $P = 0.2400$). **c**, Schematic of the experimental design. **d**, **e**, Averaged responses (left), heatmaps (middle), and AUC during 0-5 s (right) showing Ca^{2+} responses evoked by 0.4g von Frey stimulation in pre- and post-Sham 2W mice (**d**: n = 5 mice. $P = 0.4480$) and sucrose licking in pre- and post-Sham 6W mice (**e**: n = 5 mice. $P = 0.6404$). Significance was assessed by two-tailed paired Student's *t*-test in (**b**, **d**, **e**). All data are presented as the mean ± s.e.m. Not significant (ns). Details of the statistical analyses are presented in Supplementary Data 1. Created with BioRender.com (**a**, **b**, **d**, **e**).

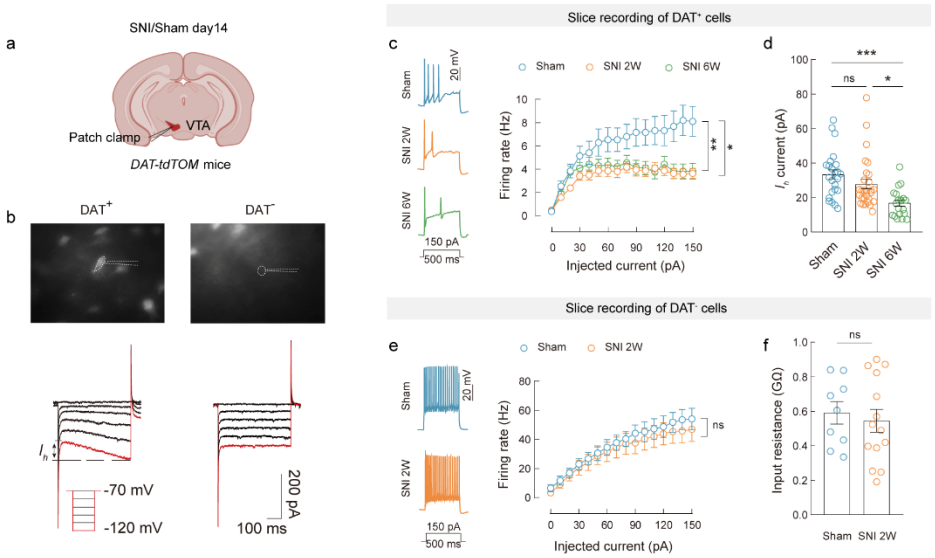

Supplementary Fig 4. The excitability of VTA neurons in SNI and Sham mice.

a, Schematic of the electrophysiological recordings in acute slices. **b**, Typical currents induced by hyperpolarizing voltage steps recorded from the DAT^+ (tdTOM positive) and DAT^- (tdTOM negative) neurons. **c**, Representative traces (left) and statistical data (right) of firing rate recorded from DAT^+ neurons of Sham, post-SNI 2W, and post-SNI 6W mice. Sham, n = 23 cells from 3 mice; SNI 2W, n = 27 cells from 3 mice; SNI 6W, n = 30 cells from 4 mice. Sham vs SNI 2W $P = 0.0056$; Sham vs SNI 6W $P = 0.0112$. **d**, Statistical data of hyperpolarization-activated currents (I_h) at -120 mV recorded from DAT^+ neurons. Sham, n = 24 cells from 3 mice; SNI 2W, n = 28 cells from 3 mice; SNI 6W, n = 20 cells from 3 mice. Sham vs SNI 2W $P = 0.3945$; Sham vs SNI 6W $P = 0.0002$; SNI 2W vs SNI 6W $P = 0.0151$. **e**, Representative traces and statistical data of firing rate recorded from DAT^- neurons of post-SNI 2W and Sham mice. Sham, n = 8 cells from 3 mice; SNI 2W, n = 11 cells from 3 mice. $P > 0.9999$. **f**, Statistical data for input resistance recorded from DAT^- neurons of post-SNI 2W and Sham mice. Sham, n = 9 cells from 3 mice; SNI 2W, n = 14 cells from 3 mice. $P = 0.6418$. Significance was assessed by two-way ANOVA followed by Bonferroni's multiple comparisons test in (**c, e**), one-way ANOVA followed by Bonferroni's multiple comparisons test in (**d**), and two-tailed unpaired Student's *t*-test in (**f**). All data are presented as the mean ± s.e.m. $^*P < 0.05$, $^{**}P < 0.01$, $^{***}P < 0.001$, not significant

(ns). Details of the statistical analyses are presented in Supplementary Data 1. Created with BioRender.com (**a**).

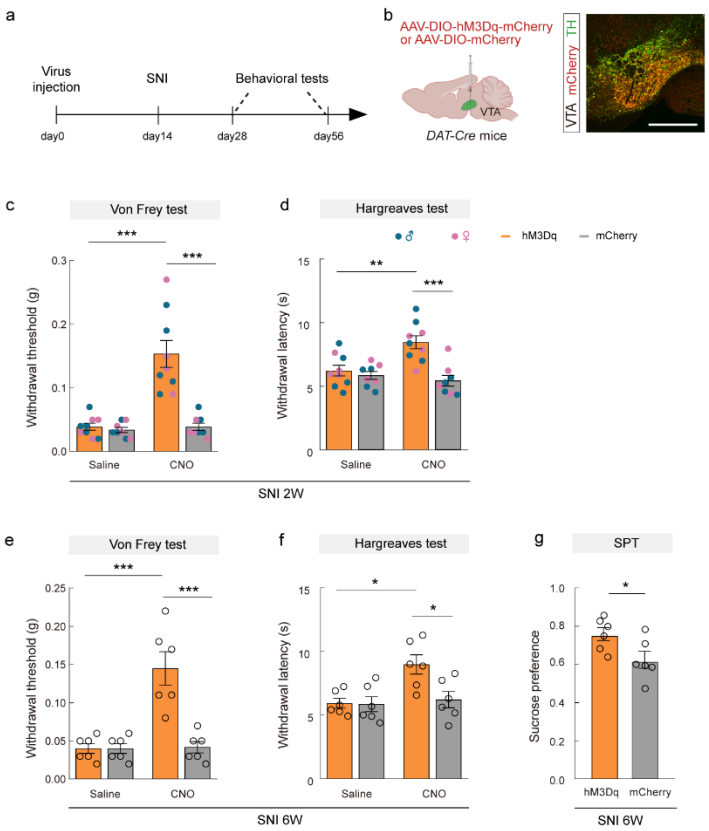

Supplementary Fig 5. Effects of chemogenetic activation of DA^{VTA} neurons on chronic pain.

a, Schematic of the experimental design. **b**, Schematic of VTA injection of AAV-DIO-hM3Dq-mCherry/AAV-DIO-mCherry (left) in *DAT*-Cre mice and representative images of mCherry-expressing neurons co-localized with TH immunofluorescence in the VTA (right). Scale bar, 500 μm. **c-f**, Statistical data for mechanical paw withdrawal threshold (**c**: hM3Dq, n = 9; mCherry, n = 8. $P < 0.0001$, **e**: hM3Dq, n = 6; mCherry, n = 6. $P < 0.0001$), thermal paw withdrawal latency (**d**: hM3Dq, n = 9; mCherry, n = 8. hM3Dq&CNO vs hM3Dq&Saline $P = 0.0045$; hM3Dq&CNO vs mCherry&CNO $P = 0.0002$, **f**: hM3Dq, n = 6; mCherry, n = 6. hM3Dq&CNO vs hM3Dq&Saline $P = 0.0115$; hM3Dq&CNO vs mCherry&CNO $P = 0.0248$), and SPT (**g**: hM3Dq, n = 6; mCherry, n = 6. $P = 0.0374$) of hM3Dq-mCherry-expressing and mCherry-expressing SNI mice with saline or CNO treatment. Significance was assessed by two-way ANOVA followed by Bonferroni's

multiple comparisons test in (**c**-**f**) and two-tailed unpaired Student's *t*-test in (**g**). All data are presented as the mean ± s.e.m. **P* < 0.05, ***P* < 0.01, ****P* < 0.001. Details of the statistical analyses are presented in Supplementary Data 1. Created with BioRender.com (**b**).

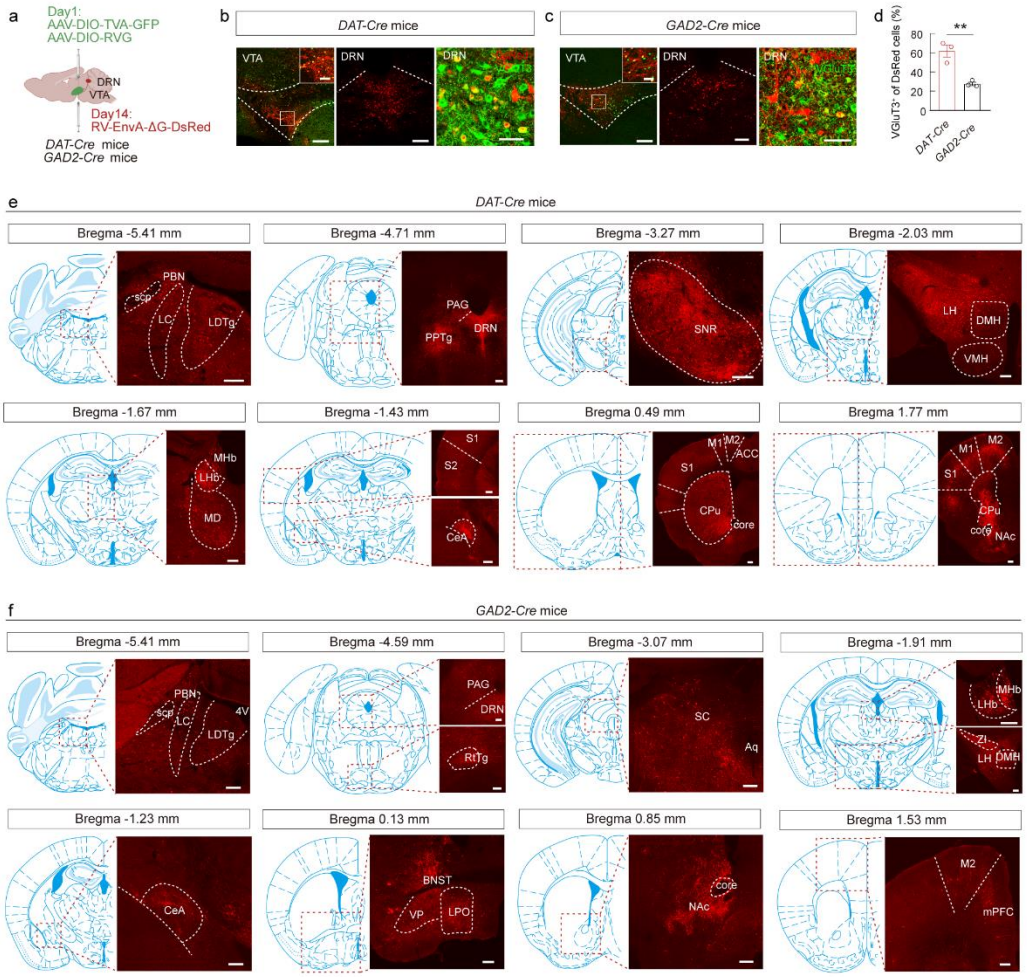

81

82 **Supplementary Fig 6. Mapping of monosynaptic inputs to DA^{VTA} and GABA^{VTA}**
83 **neurons.**

84 **a**, Schematic of the Cre-dependent retrograde monosynaptic tracing strategy in
85 *DAT-Cre* and *GAD2-Cre* mice. **b**, **c**, Representative images of the starter cells in the
86 VTA (left) and RV-DsRed-labeled cells in the DRN (middle) which co-localize with
87 VGluT3 immunofluorescence (right) from *DAT-Cre* (**b**) mice and *GAD2-Cre* mice (**c**).
88 Starter cells (yellow) co-express AAV-DIO-TVA-GFP, AAV-DIO-RVG (green), and
89 rabies RV-EnvA-ΔG-DsRed (red). Scale bars, 200 μm (left, middle) and 50 μm (upper,
90 right). **d**, Summary data for the percentage of DsRed-labeled neurons that expressed
91 VGluT3 in *DAT-Cre* and *GAD2-Cre* mice, n = 9 sections from 3 mice. $P = 0.0068$. **e**, **f**,
92 Sample images showing DsRed-expressing cells (red) that make monosynaptic inputs
93 onto DA^{VTA} neurons or GABA^{VTA} neurons. Scale bars, 200 μm. PBN, parabrachial

nucleus; LC, locus coeruleus; LDTg, laterodorsal tegmentum; PAG, periaqueductal gray; DRN, dorsal raphe nucleus; PPTg, pedunculopontine tegmentum; SNR, substantia nigra pars reticulata; LH, lateral hypothalamus; DMH, dorsomedial hypothalamus; VMH, ventromedial hypothalamus; LHb, lateral habenular nucleus; MHb, medial habenular nucleus; MD, mediodorsal thalamic nucleus; CeA, central nucleus of the amygdala; CPu, caudate putamen; S1, primary somatosensory cortex; S2, secondary somatosensory cortex; M1, primary motor cortex; M2, secondary motor cortex. ACC, anterior cingulate cortex; NAc, nucleus accumbens; BNST, bed nucleus of the stria terminalis; RtTg, reticulotegmental nucleus of the pons; ZI, zona incerta; SC, superior colliculus; VP, ventral pallidum; LPO, lateral preoptic area; mPFC, medial prefrontal cortex. Significance was assessed by two-tailed unpaired Student's *t*-test in (**d**). Data in (**d**) are presented as the mean ± s.e.m. $^{**}P < 0.01$. Details of the statistical analyses are presented in Supplementary Data 1. Created with BioRender.com (**a**).

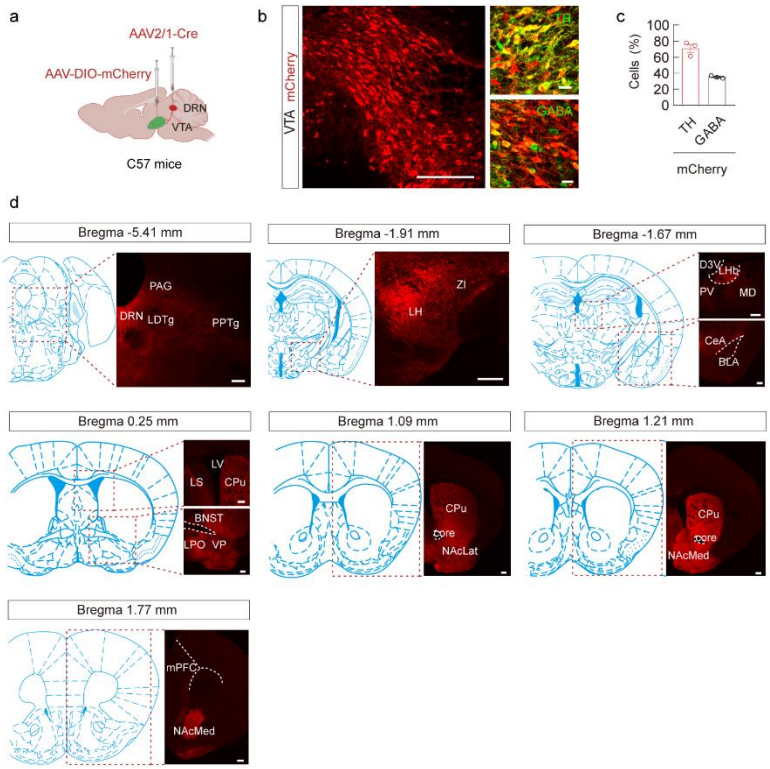

Supplementary Fig 7. Cre-dependent anterograde trans-monosynaptic tracing of DRN neurons.

a, Schematic of the Cre-dependent anterograde trans-monosynaptic tracing strategy in *C57* mice. **b**, Typical images showing mCherry expression within the VTA. Scale bars, 200 μm (left) and 100 μm (right). **c**, Summary data for the percentage of mCherry-labeled neurons co-localized with TH and GABA immunofluorescence within the VTA, n = 6 sections from 3 mice (right). **d**, Neural terminals expressing mCherry in different brain regions. Scale bars, 200 μm. PBN, parabrachial nucleus; LDTg, laterodorsal tegmentum; PAG, periaqueductal gray; DRN, dorsal raphe nucleus; PPTg, pedunculopontine tegmentum; LH, lateral hypothalamus; ZI, zona incerta; LHb, lateral habenular nucleus; PV, paraventricular thalamic nucleus; MD, mediodorsal thalamic nucleus; BLA, basolateral amygdala; CeA, central nucleus of the amygdala; LS, lateral septal nucleus; CPu, caudate putamen; LPO, lateral preoptic area; BNST, bed nucleus of the stria terminalis; VP, ventral pallidum; NAcLat, NAc lateral shell; NAcMed, NAc medial shell; mPFC, medial prefrontal cortex. Data in (**c**) are

presented as the mean ± s.e.m. Created with BioRender.com (**a**).

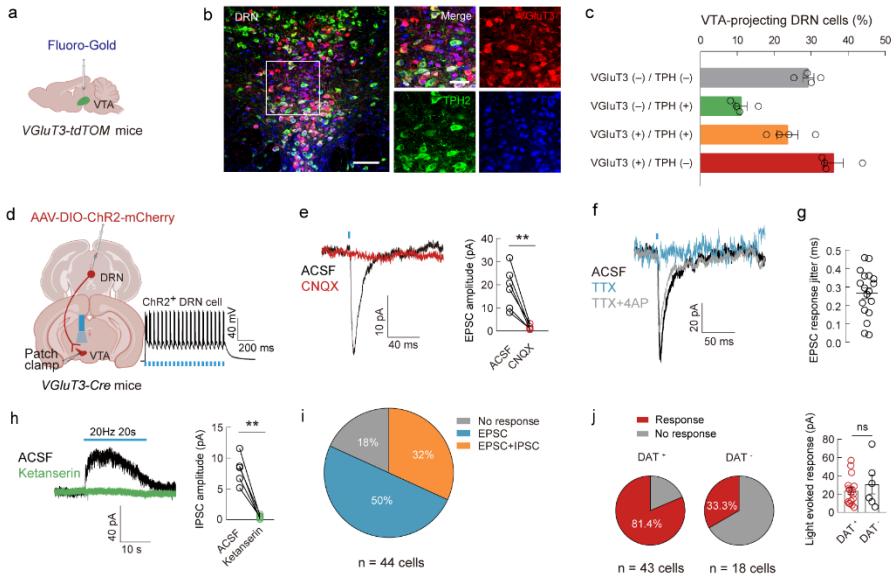

125

126 **Supplementary Fig 8. Dopamine neurons are the primary postsynaptic target of**
127 **the VGluT3^{DRN} neurons.**

128 **a**, Schematic diagram of retrograde tracer FG injected into the VTA. **b**, Typical
129 images of the FG (blue) neurons co-localize with TPH2 immunofluorescence (green)
130 in the DRN of *VGluT3-tdTOM* mice. Scale bars, 100 μm (left) and 50 μm (right). **c**,
131 Percentage of FG-labeled neurons that expressed VGluT3 and TPH2 in the DRN, n =
132 15 sections from four mice. **d**, Schematic showing viral injection and VTA
133 electrophysiological recordings in acute slices from *VGluT3-Cre* mice (left). Viral
134 expression efficacy proved by light (473 nm, 20 Hz)-evoked action potentials of
135 ChR2-mCherry-expressing neuron (right). **e**, Representative traces and summary data
136 for light-evoked EPSCs of VTA neurons before (ACSF) and after CNQX (10 μM)
137 treatment. n = 6 cells from 3 mice. P = 0.0040. **f**, Representative traces of
138 light-evoked EPSCs of the VTA neurons before (ACSF) and after TTX (1 μM) or
139 TTX and 4-AP (100 μM) treatment. **g**, Summary data for the jitter of light-evoked
140 EPSCs recorded from VTA neurons. n = 18 cells from 3 mice. **h**, Representative
141 traces and summary data for light-evoked (473 nm, 20 s, 20 Hz) slow IPSCs of VTA
142 neurons before and after ketanserin (10 μM) treatment. n = 5 cells from 3 mice. P =
143 0.0019. **i**, Pie chart showing the distribution of light-evoked response types in

DRN-targeted VTA neurons. n = 44 cells from 5 mice. **j**, Summary data for the percentage (left: DAT^+, n = 43 cells from 5 mice; DAT^-, n = 18 cells from 3 mice) and amplitudes (right: DAT^+, n = 17 cells from 4 mice; DAT^-, n = 6 cells from 3 mice. P = 0.4247) of light-evoked fast EPSCs recorded from DAT^+ and DAT^- neurons. Significance was assessed by two-tailed paired Student's *t*-test in (**e**, **h)**, and two-tailed unpaired Student's *t*-test in (**j**). All data are presented as the mean ± s.e.m. $^{**}P < 0.01$, not significant (ns). Details of the statistical analyses are presented in Supplementary Data 1. Created with BioRender.com (**a**, **d**).

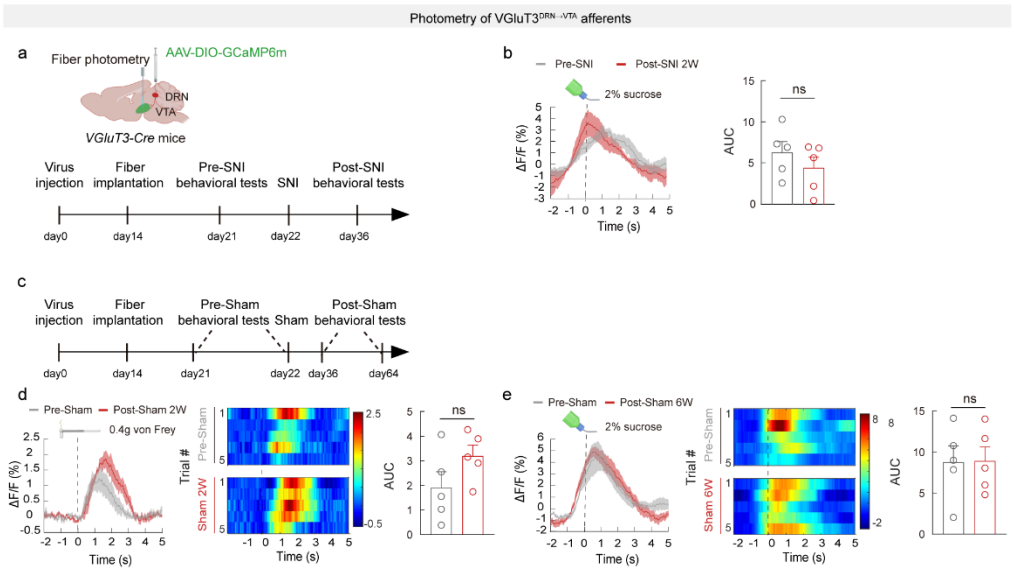

Supplementary Fig 9. Ca^{2+} signal of $VGluT3^{DRN→VTA}$ afferents.

a, Schematic of the experimental design and schematic diagram of fiber photometry of *VGluT3-Cre* mice. **b**, Averaged responses (left) and AUC during 0-5 s (right) showing Ca^{2+} responses evoked by sucrose licking in pre- and post-SNI 2W mic. $P = 0.2607$. **c**, Schematic of the experimental design. **d**, **e**, Averaged responses (left), heatmaps (middle), and AUC during 0-5 s (right) showing Ca^{2+} responses evoked by 0.4g von Frey stimulation in pre- and post-Sham 2W mice (**d**: $P = 0.1247$) and sucrose licking in pre- and post-Sham 6W mice (**e**: $P = 0.9502$). n = 5 mice per group in panels (**b**, **d**, **e**).Significance was assessed by two-tailed unpaired Student's *t*-test in (**b**, **d**, **e**). All data are presented as the mean ± s.e.m. Not significant (ns). Details of the statistical analyses are presented in Supplementary Data 1. Created with BioRender.com (**a**, **b**, **d**, **e**).

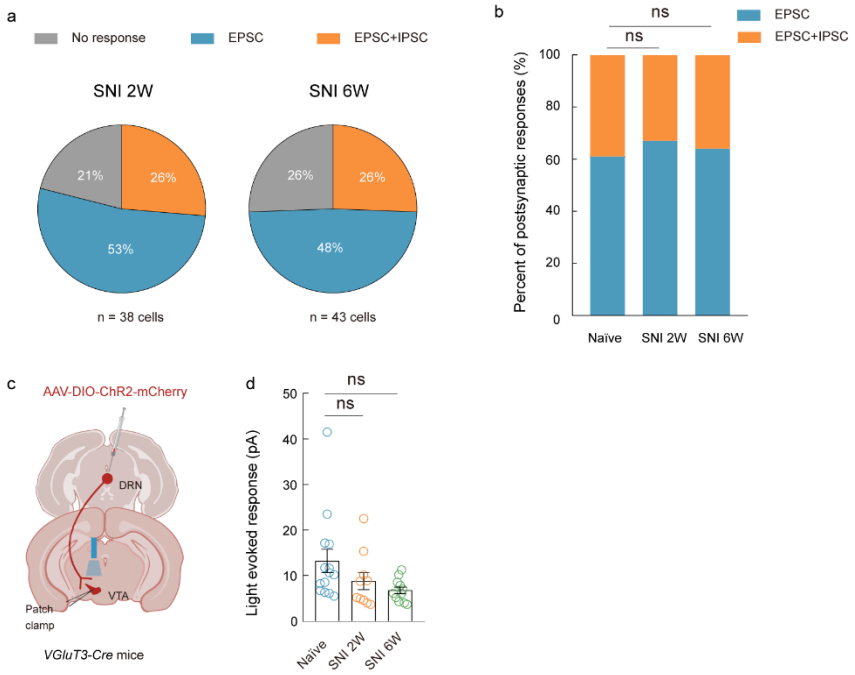

Supplementary Fig 10. Analysis of nerve injury-induced changes in the postsynaptic responses of VGluT3^{DRN}-targeted VTA neurons.

a, Pie chart showing the distribution of light-evoked response types in VGluT3^{DRN}-targeted VTA neurons of post-SNI 2W and post-SNI 6W mice. naïve vs SNI 2W P = 0.8502; naïve vs SNI 6W P = 0.6552. **b**, A bar graph illustrating the percentage of EPSC-type and EPSC+IPSC-type responses in all postsynaptic responses recorded from naïve (n = 44 cells from 5 mice), post-SNI 2W (n = 38 cells from 4 mice) and 6W mice (n = 43 cells from 4 mice). naïve vs SNI 2W P = 0.4615; naïve vs SNI 6W P = 0.7703. **c**, Schematic showing viral injection and the electrophysiological recordings in acute slices from *VGluT3-Cre* mice. **d,** Statistical data for the amplitudes of light-evoked slow IPSCs in VGluT3^{DRN}-targeted VTA neurons. (naïve, n = 14 cells from 3 mice; post-SNI 2W, n = 10 cells from 3 mice; post-SNI 6W, n = 11 cells from 3 mice. naïve vs SNI 2W P = 0.2866; naïve vs SNI 6W P = 0.0609). Significance was assessed by two-tailed Chi-square test between groups in (**a**), two-tailed Fisher's exact test in (**b**), and one-way ANOVA followed by Bonferroni's multiple comparisons test in (**d**). All data are presented as the mean ±

s.e.m. Not significant (ns). Details of the statistical analyses are presented in Supplementary Data 1. Created with BioRender.com (**c**).

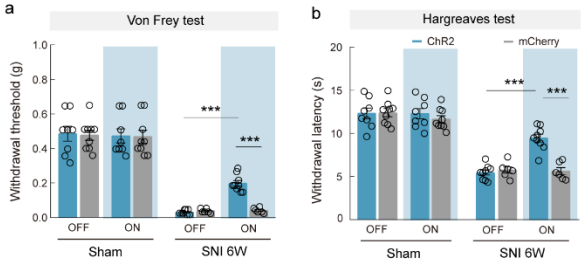

185

186 **Supplementary Fig 11. VGluT3^{DRN}→DA^{VTA} circuit contributes to analgesic effects**
187 **in post-SNI 6W mice.**

188 **a**, **b**, Mechanical paw withdrawal threshold (**a**: ChR2&ON vs ChR2&OFF $P < 0.0001$;
189 ChR2&ON vs mCherry&ON $P < 0.0001$) and thermal paw withdrawal latency (**b**:
190 ChR2&ON vs ChR2&OFF $P < 0.0001$, ChR2&ON vs mCherry&ON $P < 0.0001$) of
191 ChR2-mCherry-expressing and mCherry-expressing Sham or post-SNI 6W mice with
192 (on) or without (off) optogenetic stimulation. Sham&ChR2, n = 8; Sham&mCherry, n
193 = 9; SNI&ChR2, n = 9; SNI&mCherry, n = 6. Significance was assessed by two-way
194 ANOVA followed by Bonferroni's multiple comparisons test in (**a**, **b**). All data are
195 presented as the mean ± s.e.m. ***$P < 0.001$, not significant (ns). Details of the
196 statistical analyses are presented in Supplementary Data 1.

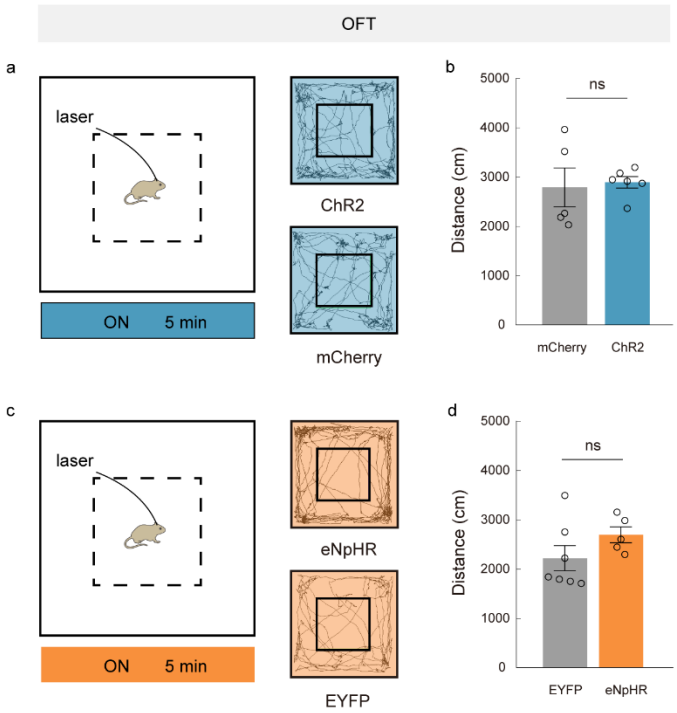

Supplementary Fig 12. Motor activity in mice with light stimulation of VGluT3$^{DRN→VTA}$ afferents.

a, **c** Experimental design (left) and representative trajectories (right) of animals expressing ChR2/mCherry (**a**) or eNpHR/EYFP (**c**) in VGluT3^{DRN} neurons during VTA light stimulation. **b**, **d**, Mean distance of ChR2/mCherry-expressing (**b**: ChR2, n = 6; mCherry, n = 5. $P = 0.7904$) and eNpHR/EYFP-expressing (**d**: eNpHR, n = 5; EYFP, n = 7. $P = 0.1855$) mice with 20 Hz optostimulationin OFT. Significance was assessed by two-tailed unpaired Student's *t*-test in (**b**, **d**). All data are presented as the mean ± s.e.m. Not significant (ns). Details of the statistical analyses are presented in Supplementary Data 1.

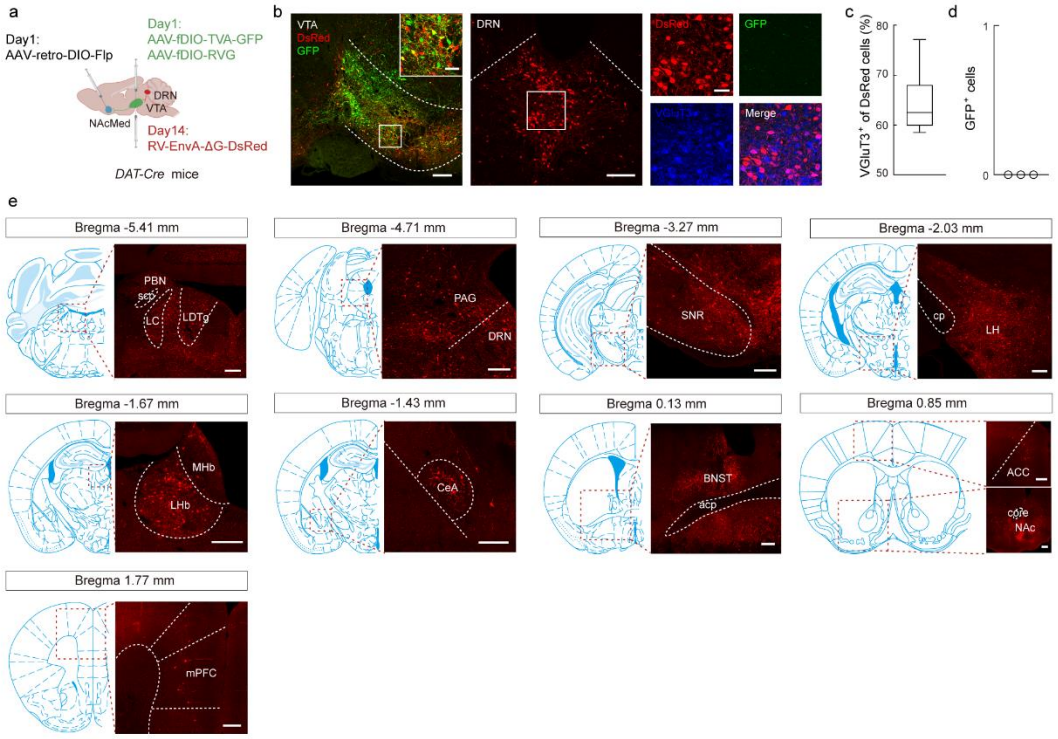

209

210 **Supplementary Fig 13. Presynaptic input to NAcMed-projecting DA^{VTA} neurons**
211 **revealed by cTRIO-based mediated trans-synaptic tracing.**

212 **a**, Schematic of cTRIO based retrograde monosynaptic tracing using *DAT-Cre* mice. **b**,
213 Representative images of the starter cells in the VTA (left) and RV-DsRed-labeled
214 cells in the DRN (middle) which co-localize with VGluT3 immunofluorescence
215 (right). Starter cells (yellow) co-expressing AAV-fDIO-TVA-GFP, AAV-fDIO-RVG
216 (green), and rabies RV-EnvA-ΔG-DsRed (red). Scale bars, 50 μm (upper) and 200 μm
217 (bottom). **c**, Percentage of DsRed-labeled neurons in the DRN that express VGluT3 in
218 *DAT-Cre* mice, n = 9 sections from three mice. **d**, GFP-expressing neurons in the
219 DRN. n = 3 mice. **e**, Representative images showing DsRed-expressing cells (red) that
220 make monosynaptic contact onto NAcMed-projecting DA^{VTA} neurons. Scale bars, 200
221 μm. PBN, parabrachial nucleus; LC, locus coeruleus; LDTg, laterodorsal tegmentum;
222 PAG, periaqueductal gray; DRN, dorsal raphe nucleus; SNR, substantia nigra pars
223 reticulata; LH, lateral hypothalamus; LHb, lateral habenular nucleus; MHb, medial
224 habenular nucleus; CeA, central nucleus of the amygdala; BNST, bed nucleus of the
225 stria terminalis; ACC, anterior cingulate cortex; NAc, nucleus accumbens; mPFC,

medial prefrontal cortex. Data in (**c**) are shown as box and whisker plots (medians, quartiles (boxes), and ranges minimum to maximum (whiskers). Created with BioRender.com (**a**).

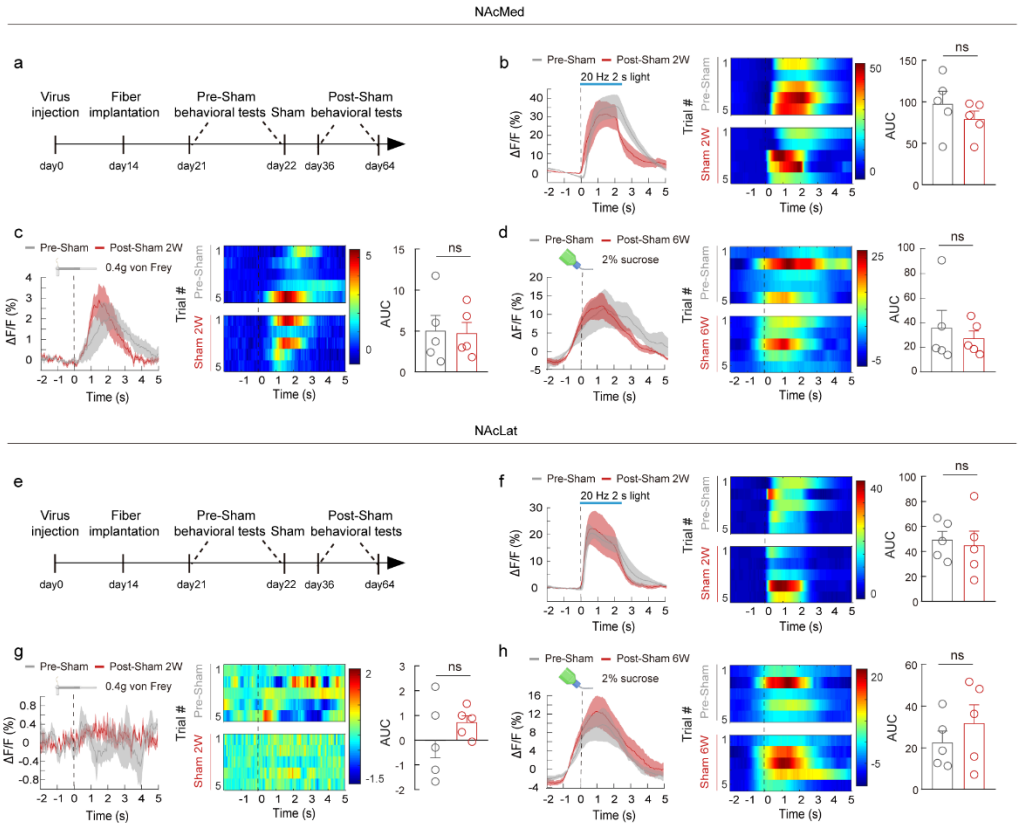

229

230 **Supplementary Fig 14. DA2m signals evoked by optogenetic activation of**
231 **VGlut3$^{DRN→VTA}$ terminals in sham mice.**

232 **a**, **e**, Schematic of the experimental design. **b-d**, **f-h**, Averaged responses (left),
233 heatmaps (middle), and AUC during 0-5 s (right) showing DA2m signals evoked by
234 optogenetic activation of VGlut3$^{DRN→VTA}$ terminals (**b**: $P = 0.1252$, **f**: $P = 0.8037$) and
235 0.4g von Frey stimulation (**c**: $P = 0.8496$, **g**: $P = 0.4663$) in pre- and post-Sham 2W
236 mice, sucrose licking in pre- and post-Sham 6W mice (**d**: $P = 0.5096$, **h**: $P = 0.3273$).
237 NAcMed group, n = 5; NAcLat group, n = 5. Significance was assessed by two-tailed
238 paired Student's *t*-test in (**b-d**, **f-h**). All data are presented as the mean ± s.e.m. Not
239 significant (ns). Details of the statistical analyses are presented in Supplementary Data
240 1. Created with BioRender.com (**c**, **d**, **g**, **h**).

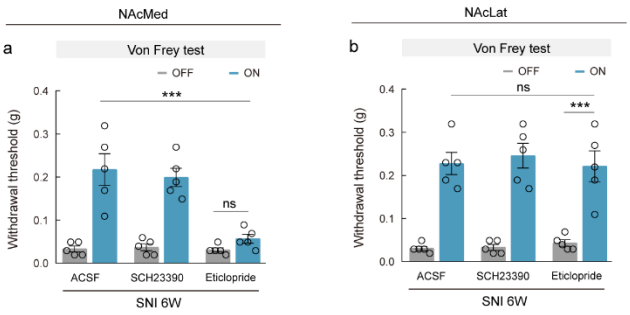

241

242 **Supplementary Fig 15. D2 receptors within NAcMed contribute to pain relief**
243 **through VGluT3^{DRN}→DA^{VTA} circuit in post-SNI 6W mice.**

244 **a**, **b**, Effects of optogenetic activation of VGluT3$^{DRN→VTA}$ terminals on punctate
245 mechanical hypersensitivity with drug infusion into the NAcMed (**a**: ACSF&ON vs
246 Eticlopride&ON $P < 0.0001$; Eticlopride&ON vs Eticlopride&OFF $P > 0.9999$) or
247 NAcLat (**b**: ACSF&ON vs Eticlopride&ON $P > 0.9999$; Eticlopride&ON vs
248 Eticlopride&OFF $P < 0.0001$) in post-SNI 6W mice. NAcMed group, n = 5; NAcLat
249 group, n = 5. Significance was assessed by two-way ANOVA followed by
250 Bonferroni's multiple comparisons test. All data are presented as the mean ± s.e.m.
251 ***$P < 0.001$, not significant (ns). Details of the statistical analyses are presented in
252 Supplementary Data 1.

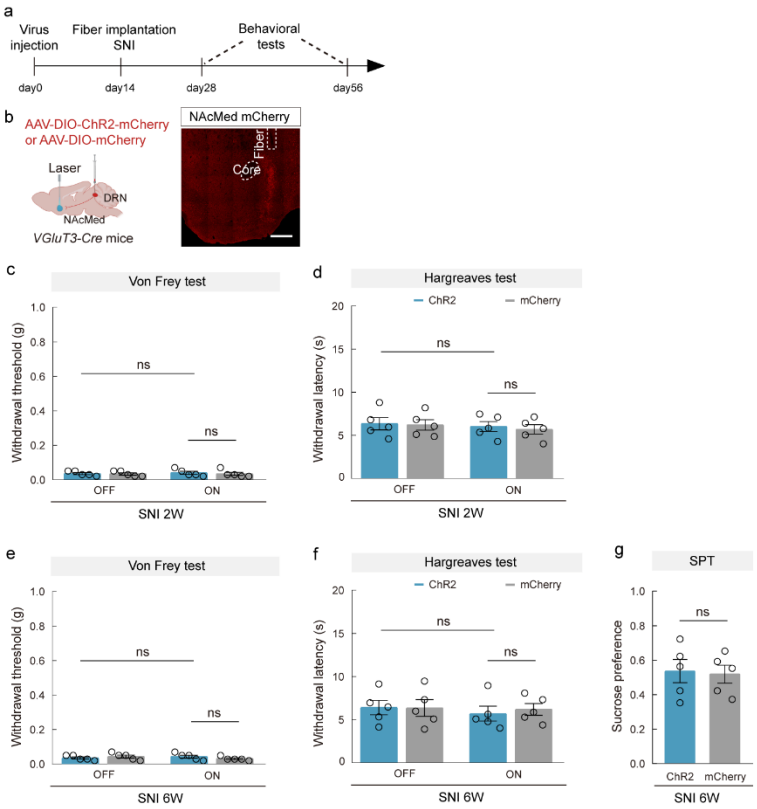

253

254 **Supplementary Fig 16. Effects of activation of VGluT3^{DRN} neural terminals**
255 **within the NAcMed on chronic pain hypersensitivity and CAB.**

256 **a,** Schematic of the experimental design. **b**, Schematic of DRN injection of
257 AAV-DIO-ChR2-mCherry/AAV-DIO-mCherry and representative images showing
258 NAcMed optical fiber implantation in *VGluT3*-Cre mice. Scale bars, 500 μm. **c-f**,
259 Mechanical paw withdrawal threshold (**c**: ChR2&ON vs ChR2&OFF $P > 0.9999$;
260 ChR2&ON vs mCherry&ON $P > 0.9999$, **e**: ChR2&ON vs ChR2&OFF $P > 0.9999$;
261 ChR2&ON vs mCherry&ON $P > 0.9999$) and thermal paw withdrawal latency (**d**:
262 ChR2&ON vs ChR2&OFF $P > 0.9999$; ChR2&ON vs mCherry&ON $P > 0.9999$, **f**:
263 ChR2&ON vs ChR2&OFF $P > 0.9999$; ChR2&ON vs mCherry&ON $P > 0.9999$) of
264 ChR2-mCherry-expressing and mCherry-expressing SNI mice with (on) or without
265 (off) optogenetic stimulation. **g**, Preference for sucrose in the SPT, $P = 0.8377$. n = 5
266 mice per group in panels (**c-g**). Significance was assessed by two-way ANOVA
267 followed by Bonferroni's multiple comparisons test in (**c-f**) and two-tailed unpaired
268 Student's *t*-test in (**g**). All data are presented as the mean ± s.e.m. Not significant (ns).

Details of the statistical analyses are presented in Supplementary Data 1. Created with BioRender.com (**b**).

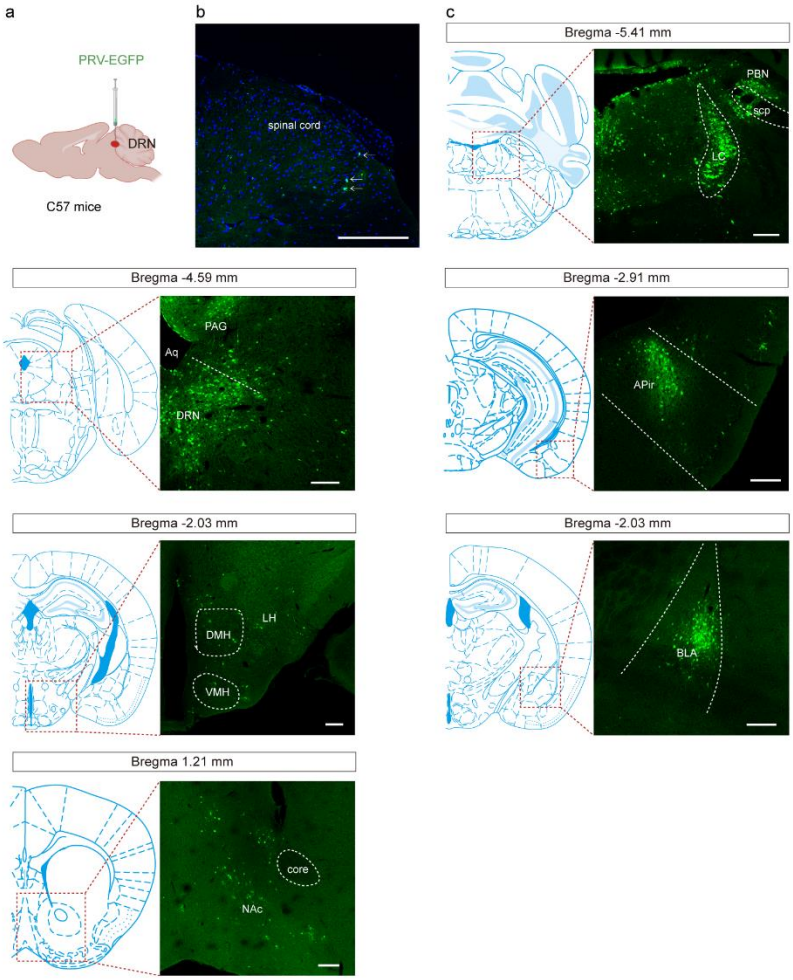

271

272 **Supplementary Fig 17. Retrograde and trans-synaptic tracing of DRN-upstream**
273 **neurons with PRV-EGFP injection.**

274 **a**, Schematic of the retrograde and trans-synaptic tracing strategy using PRV-EGFP in
275 *C57* mice. **b**, EGFP-expressing neurons detected in the spinal dorsal horn. Scale bars,
276 200 μm. **c**, Sample images showing EGFP-expressing cells (green) that make
277 trans-synaptic inputs onto DRN neurons. Scale bars, 200 μm. PBN, parabrachial
278 nucleus; PAG, periaqueductal gray; LC, locus coeruleus; DRN, dorsal raphe nucleus;
279 APir, amygdalopiriform transition area; LH, lateral hypothalamus; DMH, dorsomedial
280 hypothalamus; VMH, ventromedial hypothalamus; BLA, basolateral amygdala; NAc,
281 nucleus accumbens. Created with BioRender.com (**a**).

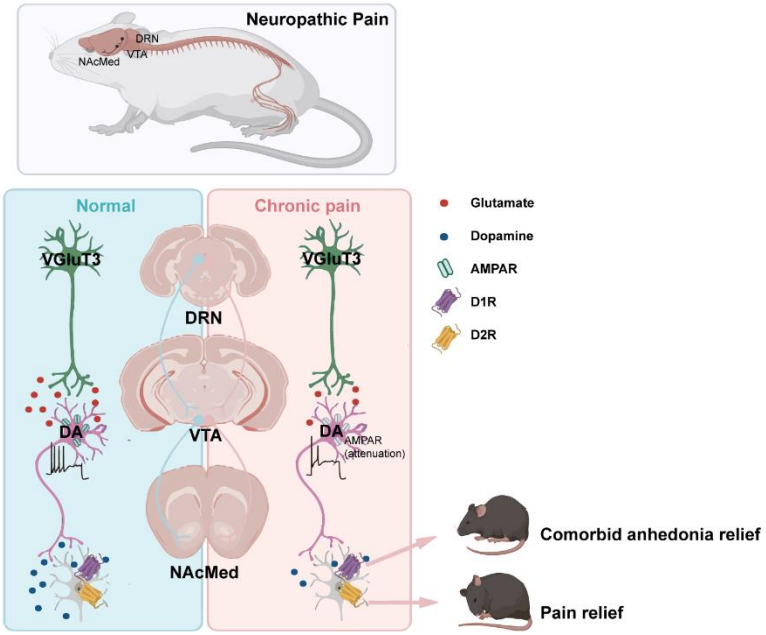

Supplementary Fig 18. Schematic summary of maladaptive changes of VGluT3^{DRN}→DA^{VTA}→D1/D2^{NAcMed} circuit during neuropathic pain.

In the chronic pain state, the VGluT3^{DRN}→DA^{VTA} circuit undergoes decreased presynaptic glutamate release and undermined postsynaptic response to glutamate, leading to hypoexcitability of DA^{VTA} neurons and thus reducing dopamine release into the NAcMed. Gain-of-function of VGluT3^{DRN}→DA^{VTA} circuit efficiently relieves neuropathic pain and comorbid anhedonia-like behavior via D2R and D1R in the NAcMed, respectively. Created with BioRender.com.

291